Improving NO₂ and ozone simulations through global NOₓ emission inversions

Zhen Qu[1,2], Daven K. Henze[1], Owen R. Cooper[3,4], Jessica L. Neu[5]

[1]Department of Mechanical Engineering, University of Colorado Boulder, Boulder, CO, 80309, USA
5 [2]School of Engineering and Applied Science, Harvard University, Cambridge, MA, 02138, USA
[3]Cooperative Institute for Research in Environmental Sciences, University of Colorado, Boulder, CO, 80309, USA
[4]NOAA Chemical Sciences Laboratory, Boulder, CO, 80305, USA
[5]Jet Propulsion Laboratory, California Institute of Technology, Pasadena, CA, 91109, USA

10 *Correspondence to*: Zhen Qu (zhen.qu@colorado.edu)

Abstract. Tropospheric ozone simulations have large uncertainties, but their biases, seasonality and trends can be improved with more accurate estimates of precursor gas emissions. We perform global top-down estimates of monthly NOₓ emissions using two OMI NO₂ retrievals (NASAv3 and DOMINOv2) from 2005 to 2016 through a hybrid 4D-Var / mass balance inversion. The 12-year averages of regional NOₓ budgets from the NASA posterior emissions are 37% to 53% smaller than

15 the DOMINO posterior. Compared to surface NO₂ measurements, GEOS-Chem adjoint NO₂ simulations using the DOMINO posterior NOₓ emissions have smaller biases in China (by 15%) and the US (by 22%), but NO₂ trends have more consistent decreases (by 26%) with the measurements (by 32%) in the US from 2006 to 2016 when using the NASA posterior. The two posterior NOₓ emissions datasets have different strengths with respect to simulation of ozone concentrations. Simulations using NASA-based emissions provide better agreement for polluted conditions. Ozone from

20 these shows the highest correlation ($R^2 = 0.88$) with annual MDA8 ozone trends and alleviates the double peak in the prior simulation of global ozone seasonality. The DOMINO-based emissions, on the other hand, are better for simulating ozone at remote sites, making them well-suited to generation of boundary conditions for regional models, and in capturing the interannual variability of daytime-average ($R^2 = 0.72 - 0.81$) and 24-hour average ($R^2 = 0.88 - 0.96$) surface ozone. We recommend using NOₓ emission datasets that have the best performance in the corresponding spatial domain and temporal

25 focus to improve ozone simulations.

1 Introduction

Tropospheric ozone is a harmful secondary air pollutant affecting human health, sensitive vegetation, and ecosystems [NRC, 1991; Monks et al., 2015]. Long-term ozone (O₃) exposure is estimated to cause 1.04 – 1.23 million respiratory deaths in adults [Malley et al., 2017]. Short-term exposure to high ambient ozone is associated with respiratory and cardiovascular

30 mortality [Turner et al., 2016; Fleming et al., 2018]. Accurate simulations of ozone in highly polluted regions are important for better pollution forecasts and more effective emission regulations. Tropospheric ozone is formed through photochemical

reactions between nitrogen oxide (NO_x = NO + NO_2), carbon monoxide (CO), methane (CH_4), and volatile organic compounds (VOCs) in the presence of sunlight [Crutzen, 1973; Derwent et al., 1996]. These precursor gases are mainly emitted from fossil fuel combustion, biomass burning, oil and gas production, industry, agriculture, and biogenic activities.

35 Tropospheric ozone can also be transported from the stratosphere through stratosphere-troposphere exchange [Stohl et al., 2003; Hsu and Prather, 2009; Stevenson et al., 2006], but this magnitude is smaller than the amount from chemical production by a factor of 5 – 7 [Young et al., 2013]. Ozone is removed from the troposphere through deposition [Fowler et al., 2009], photo-dissociation, and reactions with HO_2, NO_2, unsaturated VOCs, halogens, and aerosols [Crutzen, 1973].

40 From 1850 to 2000, global mean tropospheric ozone burden has increased by 29% [Young et al., 2013]. Human activities are major sources of ozone precursor gases, contributing to 9% (24.98 Tg) increase of the global tropospheric ozone burden from 1980 to 2010 [Zhang et al., 2016]. Ozone formations and trends depend nonlinearly on the local relative abundances of NO_x and VOCs. Previous studies have shown that changes in surface ozone are dominated by regional emission trends of precursor gases [Zhang et al., 2016]. At the global scale, 77% of NO_x emissions are from anthropogenic sources, according 45 to the HTAP 2010 inventory [Janssens-Maenhout, 2015]. Anthropogenic NO_x emissions have been decreasing in North America and Europe due to transportation and energy transformations [Simon et al., 2015], but have been increasing in China up until 2011 according to bottom-up emission inventories [Liu et al., 2016; Hoesly et al., 2018]. Top-down NO_x emission estimates using satellite observations from the Ozone Monitoring Instrument (OMI) showed a similar turning point in China [Miyazaki et al., 2017; Qu et al., 2017], but a slowdown in reductions in the US compared to bottom-up estimates 50 [Miyazaki et al., 2017; Jiang et al., 2018]. However, in India and the Middle East, where ozone production is more efficient than higher latitude regions [Zhang et al., 2016], NO_2 column densities from OMI are continuing to increase [Krotkov et al., 2016].

Top-down methods have the advantage of being able to update emissions in a more timely fashion than the bottom-up 55 approaches; still, top-down approaches can contain large differences and uncertainties. For instance, the magnitude of tropospheric NO_2 column densities from two global retrievals from the National Aeronautics and Space Administration (NASA) and the Royal Netherlands Meteorological Institute (KNMI) differ by 50%, and have different trends at the regional scale [Zheng et al., 2014; Canty et al., 2015; Qu et al., 2017]. These differences in column densities can propagate to differences in top-down NO_x emission estimates [e.g., Miyazaki et al., 2017; Qu et al., 2017]. In this study, we assess the 60 importance of these discrepancies in NO_x emissions for the simulation of ozone. We derive global top-down NO_x emissions from 2005 to 2016 using two widely used products (OMNO2 v3 and Dutch OMI NO_2 (DOMINO) v2) based on the same inversion process for consistent evaluations (Sect. 3). We also evaluate a new OMI NO_2 retrieval product, the Quality Assurance for the Essential Climate Variables (QA4ECV) [Boersma et al., 2018], and apply it to derive monthly NO_x emissions in 2010. We do not repeat our entire set of ozone evaluations with this product given that its magnitude and 65 seasonality does not significantly different from the other two products. We further explore the impact of adjusting NO_x

emissions on ozone simulations, by evaluating the ozone simulations produced from bottom-up and top-down NO_x emissions against global surface measurements from the Tropospheric Ozone Assessment Report (TOAR) database and the China National Environmental Monitoring Center (CNEMC) network.

70   In addition to local sources, the lifetime of ozone (~22 days on global average) is sufficiently long enough for intercontinental transport [UNECE, 2010]. Consequently, every country is an exporter as well as an import of ozone pollution. Transport from East Asia can be an important contributor to ozone exceedances in the western US [Goldstein et al., 2004; Zhang et al., 2009; Zhang et al., 2014; Fiore et al., 2014; Verstraeten et al., 2015; Lin et al., 2017; Jaffe et al., 2018]. The influence of intercontinental ozone transport is strongest in spring and summer, when background ozone concentrations

75   reach 50 ppbv at the west coast of the US [Jaffe et al., 2018]. The impact of background ozone is increasingly important and challenging due to the decreased local sources of precursor gases in the US [Hoesly et al., 2018] and the recent stricter ozone standard in the US lowering the annual 4th highest maximum daily 8-hour average ozone concentration from 75 ppbv to 70 ppbv in 2015 [Cooper et al., 2015]. Optimization of NO_x emissions in the upwind regions can potentially improve remote ozone simulations in downwind regions after transport of intercontinental pollution plumes from the free troposphere to the

80   surface. Therefore, we also evaluate the model simulations of remote ozone at the west coast of the United States using bottom-up and top-down NO_x emissions in Sect. 4.

2 Methods

2.1 GEOS-Chem and its adjoint model

The GEOS-Chem adjoint model [Henze et al., 2007] v35k is used to derive global NO_x emission estimates at 2° × 2.5°

85   resolution. It was developed for inverse modeling of aerosol and gas emissions using the 4D-Var method by Henze et al. [2007, 2009] based on version 8 of GEOS-Chem, with bug fixes and updates up to version 10. Simulations in this study are driven by Modern-Era Retrospective analysis for Research and Applications, Version 2 (MERRA-2) meteorological fields from NASA Global Modeling and Assimilation Office (GMAO). Anthropogenic emissions of NO_x, SO_2, NH_3, CO, NMVOCs and primary aerosol from the HTAP 2010 inventory version 2 [Janssens-Maenhout et al., 2015] are used to drive

90   all prior simulations from 2005 to 2017. The use of non-anthropogenic emissions and other setups follow Qu et al. [2017, 2019]. In the following analyses, we refer to this model as "GC-adj."

GC-adj does not include several halogen chemistry mechanisms that affect ozone depletions primarily over the oceans [Sherwen et al., 2016a; Wang et al., 2019] and at high altitude regions [Sherwen et al., 2016a]. Given their impact on the

95   global background ozone concentrations, we also use GEOS-Chem v12.1.1 to evaluate ozone simulations at 2° × 2.5° resolution driven by the MERRA-2 meteorological fields. The chemistry updates include the stratospheric chemistry from the Universal tropospheric-stratospheric Chemistry eXtension (UCX) [Eastham et al., 2014], halogen chemistry [Bell et al.,

2002; Parrella et al., 2012; Sherwen et al., 2016a, 2016b; Schmidt et al., 2016; Sherwen et al., 2017], and updated isoprene and monoterpene chemistry [Chan Miller et al., 2017; Fisher et al., 2016; Marais et al., 2016; Travis et al., 2016]. The

100   Harvard-NASA Emission Component (HEMCO) is employed to process emissions in this version of GEOS-Chem [Keller et al., 2014]. We use 72 levels of vertical grid and global anthropogenic emissions from the Community Emissions Data System (CEDS) [Hoesly et al., 2018]. Top-down NO_x emissions derived using GC-adj are also input to this model to evaluate the impact of NO_2 data assimilation on ozone simulations under different chemical mechanisms. We refer to this model as "GCv12" in this manuscript.

105

To avoid high biases when comparing simulated ozone averaged over the first vertical model layer (~100 m in box height) with surface measurements, 2-meter ozone mixing ratios are calculated by scaling simulated ozone mixing ratios in the first layer using adjusted dry deposition velocities at 2 meters following Zhang et al. [2012] and Lapina et al. [2015].

2.2 Satellite observations and global top-down NO_x emissions

110   We estimate global top-down NO_x emissions at the surface from 2005 to 2016 at 2° × 2.5° resolution using tropospheric NO_2 column densities from OMI. OMI is an Ultraviolet/Visible nadir solar backscatter spectrometer aboard the NASA Aura satellite. It has a local overpass time of about 13:45 and a nadir resolution of 13 km × 24 km. OMI was launched in July 2004 and has provided operational data products since October 2004. Two Level 2 NO_2 retrieval products are used to derive long-term top-down NO_x emissions in this study: the NASA standard product OMNO2 version 3 [Krotkov et al., 2017] and

115   the DOMINO version 2 from KNMI [Boersma et al., 2011]. A new OMI NO_2 retrieval, the Quality Assurance for the Essential Climate Variables (QA4ECV) [Boersma et al., 2018], has recently become available. This product is jointly developed by KNMI, the Belgian Institute for Space Aeronomy (BIRA-IASB), University of Bremen, Max-Plank Institute for Chemistry, and Wageningen University. We evaluate the magnitude of NO_2 column densities and the seasonality of posterior NO_x emissions in 2010 from this product. We screen all OMI NO_2 retrievals using data quality flags and by the

120   criteria of positive tropospheric column, cloud fraction < 0.2, solar zenith angle < 75°, and viewing zenith angle < 65°. The assimilation of NO_2 slant column densities (SCDs) and the hybrid 4D-Var / mass balance inversion of NO_x emissions follows Qu et al. [2017]. We use top-down NO_x emissions estimated from the NASA standard product and the DOMINO product in the evaluations of ozone simulations.

2.3 Surface measurements

125   We evaluate surface NO_2 simulations with measurements from the Environmental Protection Agency (EPA) Air Quality System (AQS) in the US and the China National Environmental Monitoring Center (CNEMC) network in China. Simulated ozone mixing ratios from 2006 to 2016 are compared to surface observations from the TOAR Surface Ozone Database [Schultz et al., 2017] at the global scale and the CNEMC network in China. TOAR has produced a relational database of global surface ozone observations at all available sites; see Gaudel et al. [2018] for illustrations of the global coverage of the

130   TOAR data. Precompiled TOAR data (https://doi.pangaea.de/10.1594/PANGAEA.876108, available from 1995 to 2014) at
        each individual site are used in this study. Given the sparse TOAR data coverage of only 32 sites over China, hourly surface
        ozone measurements from the CNEMC (http://106.37.208.233:20035/) are used to evaluate simulations in China from 2014
        to 2016. The CNEMC national network was designed for urban and suburban air pollution monitoring. The archive contains
        hourly observations of ozone, carbon monoxide, nitrogen dioxide, sulfur dioxide and fine particulate matter across mainland
135   China since 2013.

2.4 Ozonesonde measurements

        Ozone profile measurements from the Intercontinental Chemical Transport Experiment Ozonesonde Network Study (IONS-
        2010) [Cooper et al., 2011] are used to evaluate the continental inflow of ozone along the west coast of the United States,
        where air masses are not influenced by recent US emissions. IONS-2010 was a component of the California Research at the
140   Nexus of Air Quality and Climate Change (CalNex) 2010 experiment [Ryerson et al., 2013] and was a continuation of
        previous IONS experiments to measure tropospheric ozone variability across North America [Thompson et al., 2007, 2008;
        Cooper et al., 2007]. Balloon-borne electrochemical cell sensors were used to measure ozone profiles with an accuracy of +/-
        10% in the troposphere [Johnson et al., 2002; Smit et al., 2007]. All six sites in California from IONS-2010 (Trinidad Head,
        Point Reyes, Point Sur, San Nicolas, Joshua Tree, and Shasta) are included in this study. These measurements are made in
145   the mid-afternoon (95% occurring between 14:00 and 16:59 local time) over a six-week period from May 10 to June 19,
        2010. There are 34-37 profiles for all sites except for San Nicolas Island, where only 26 profiles are available due to multiple
        instrument failures. Measurements made between 700 – 800 hPa are used to evaluate remote ozone simulations.

3 Magnitude, seasonality and trend of NO_x emissions, surface NO_2 and surface ozone

3.1 Annual average

150   Differences between the prior and posterior NO_x emission estimates are mainly driven by the differences between simulated
        and retrieved tropospheric NO_2 vertical column densities (VCDs), which are compared in Sect. S1 in the supporting
        information. As shown in Table 1, the global budgets of NO_x emissions from the NASA posterior in 2010 is 0.7% smaller
        than the prior; DOMINO posterior is 18% larger than the prior; QA4ECV posterior is 11% larger than the prior. The positive
        increment in the DOMINO posterior emissions is consistent with the +26% increments of 10-year mean posterior NO_x
155   emissions in Miyazaki et al. [2017]. The annual global NO_x emissions from Miyazaki et al. [2017] are between 46.7 Tg N yr^{-1}
        and 50.9 Tg N yr^{-1} from 2005 to 2014, which are within 31% from the DOMINO posterior emissions in 2010 in this study.

        As shown in Fig. 1, the NASA posterior NO_x emissions are less than the prior NO_x emissions in the northeast US, northeast
        China, and southeast China. The DOMINO posterior NO_x emissions are larger than the prior in most regions except for
160   North Mexico and most parts of the tropics. The QA4ECV posterior NO_x emissions have more consistent negative

increments in Eastern China with the NASA posterior emissions and more consistent positive increments in the United States, India, Europe, and Australia with the DOMINO posterior emissions. At the regional scale, NASA posterior increments are -3% in China, -1% in the US, +0.3% in India, and -1% in Western Europe. The increments from the DOMINO posterior emissions are +21% in China, +31% in the US, +28% in India, and +38% in Western Europe. The

165   different changing directions in the above two posterior NO_x emissions are consistent with the reportedly higher magnitude of NO_2 column densities in the DOMINO product than the NASA product in densely populated and industrial regions [Zheng et al., 2014; Canty et al., 2015; Qu et al., 2017]. The increments from the QA4ECV posterior emissions are +5% in China, +19% in the US, +18% in India, and +14% in Western Europe.

170   To evaluate the magnitude of the posterior NO_x emissions, we compare simulations of surface NO_2 concentrations using the NASA and DOMINO based NO_x emissions with surface measurements in the US and China. Valin et al. [2011] showed negative biases in the coarse resolution simulations of NO_2 column densities due to inaccurate NO_2 - OH feedback. Therefore, NO_2 column simulations at 2° × 2.5° in this study are likely to be underestimated and lead to high biases of posterior NO_x emissions to match satellite NO_2 column concentrations. In addition to this bias in column concentration,

175   surface NO_2 simulations at coarse resolution are usually biased low compared to measurements at urban sites, due to the short lifetime of NO_x. We therefore start with analyzing this resolution error by generating high-resolution pseudo surface measurements at 0.1° × 0.1° and compare them with low-resolution model simulations at 2° × 2.5°. We generate high-resolution surface NO_2 concentrations by scaling simulated surface NO_2 concentrations at 2° × 2.5° grid cells by the ratio of OMI NO_2 column density gridded at 0.1° × 0.1° to the average of GEOS-Chem simulated NO_2 column density over 2° ×

180   2.5° grid cell. We identify 0.1° × 0.1° grid cells that include surface monitoring sites and treat downscaled surface NO_2 concentrations at these grid cells as the pseudo surface measurements. Comparisons of pseudo surface measurements and NO_2 simulations at 2° × 2.5° purely reflect differences caused by comparing NO_2 concentrations at 2° × 2.5° with higher resolution surface measurements at urban regions. The mean of the pseudo NO_2 measurements is 32% higher than the low-resolution simulations in the US, and it is 18% higher than the low-resolution simulations in China. The real surface

185   measurements, which represent a single point within the 0.1° × 0.1° grid cell, are expected to have even larger biases than the values calculated here, where we assume the measurements are at 0.1° × 0.1° grid cells. The smaller bias in China in comparison to the US is related to the higher background NO_2 concentrations in China.

Figure 2 shows the comparisons of annual mean surface NO_2 concentrations in 2015 from measurements and simulations

190   using different NO_x emission inputs. The selection of this year is due to the limited availability of nation-wide surface NO_2 measurements in China. Surface NO_2 concentrations in both China and the US are measured by chemiluminescence analyzers, each equipped with a molybdenum converter, which converts additional NO_y compounds to NO and leads to a positive bias in NO_2 measurements [Dunlea et al., 2007; Steinbacher et al., 2007]. We therefore calculate a correction factor following Lamsal et al. [2008] for each GEOS-Chem simulation and divide the simulated NO_2 concentrations by this

195   correction factor to convert simulated NO_2 to the measured species. Subtracting the resolution bias from the statistics shown on Fig. 2, the equivalent normalized mean bias (NMB) of surface NO_2 concentrations using the NASA posterior is -54% in China and -41% in the US. The equivalent NMB using the DOMINO posterior is -38% in China and -19% in the US. Although we have not performed a NO_x emission inversion using the QA4ECV product for 2015, we expect its bias to lie between the results from the NASA and DOMINO products, based on the magnitude of NO_x emissions in 2010.

200

We evaluate the simulated ozone concentrations with global surface measurements from the TOAR database using three ozone metrics: maximum daily 8-hour average (MDA8) ozone, daytime average ozone (8:00 – 20:00 local time), and 24-hour average ozone. In addition to the GC-adj simulation, with which we derived top-down NO_x emissions, we also input the same top-down emissions to GCv12 and evaluate ozone simulations from this more recent version of the GEOS-Chem that

205   includes updated halogen and isoprene chemistry.

All GC-adj simulations of 2-meter ozone concentrations have a high bias compared to the TOAR measurements in 2010. NMB and Normalized Mean Square Error (NMSE) are largest for 24-hour ozone concentrations. Simulations using posterior NO_x emissions have slightly better agreement with the measurements from TOAR in 2010 (Fig. 3). In particular, simulations

210   using the DOMINO posterior NO_x emissions have the smallest NMB in all ozone metrics and the smallest NMSE in all metrics except for the North Hemisphere (NH) summertime MDA8 ozone. Simulations using the NASA posterior NO_x emissions have the best spatial correlation when compared with measurements for all metrics except for the NH summer daytime ozone and annual MDA8 ozone, for which DOMINO posterior simulations have the largest correlation coefficient (Fig. S2).

215

In comparison, GCv12 simulations have a low bias in daytime ozone, but high bias in 24-hour average ozone, reflecting the potential underestimate of ozone loss at night. The impact of NO_2 assimilation on improving estimates of surface ozone simulations in GCv12 depends upon the ozone metric, as shown in the bottom left panel of Fig. 3. Simulations using the DOMINO posterior emissions have the smallest NMB for annual mean daytime ozone; simulations using bottom-up NO_x

220   emissions have the smallest NMB for annual mean MDA8 ozone; simulations using the NASA posterior emissions have the smallest NMB for annual mean 24-hour averaged ozone. These results suggest that the simulated diurnal variations of surface ozone concentrations may not be correct. The current constraints on NO_x emissions use observations from OMI, which overpasses the same location approximately once per day. The diurnal variations of NO_x emission are constrained to be those of the prior emissions. OMI measurements frequently miss the high values of NO_2 column densities that occur

225   before or after its overpassing time (as shown from comparisons with PANDORA measurements [Herman et al., 2019]). Future hourly constraints from the upcoming geostationary satellite data (e.g., Geo-stationary Environmental Monitoring Spectrometer (GEMS), Tropospheric Emissions: Monitoring of Pollution (TEMPO) [Zoogman et al., 2017] and Sentinel-4) have the potential to improve simulations of NO_2, ozone diurnal variations, and different ozone metrics. Simulated MDA8

ozone values are mostly biased low in NH summer but biased high in annual mean concentrations, reflecting different
230   seasonal variations in simulated and measured ozone concentrations, which will be further discussed in Sect. 3.2.
Evaluations with the CNEMC ozone measurements in China are in Sect. S2.

3.2 Seasonal variation

The seasonal variations of monthly NO_x emissions are consistent between the prior and the NASA posterior emissions (Fig.
4). The DOMINO posterior emissions show different seasonal variations in several regions. In China, the prior and the
235   NASA posterior NO_x emissions show summer peaks, which are mainly caused by the increase of natural sources when
temperatures are high and lightning occurs more often [Qu et al., 2017]. The DOMINO posterior emissions have the largest
values in January and June in China, consistent with the posterior seasonality from Miyazaki et al. [2017] constrained by the
same OMI NO_2 product. The peak of the DOMINO posterior NO_x emissions in the United States and Mexico shifted earlier
in the year to June and July compared to the prior and NASA posterior emissions, similar to the results from Miyazaki et al.
240   [2017], and could possibly be explained by better constraints on soil NO_x emissions in rural regions in the DOMINO
posterior. The differences between the DOMINO posterior and the other two sets of emissions are especially large during the
springtime in India, when biomass burning activity increases [Miyazaki et al., 2017; Venkataraman et al., 2006]. These
different seasonal variations in the posterior NO_x emissions may reflect the different sensitivity of OMI NO_2 retrievals to
NO_x sources and regions. The seasonal variations of simulated surface NO_2 concentrations are similar with measurements in
245   China and the US (see Fig. S4).

Seasonal variations of 2-meter ozone concentrations simulated by the GC-adj are also similar despite different NO_x emission
inputs: the differences in correlation coefficients of the simulated and the measured monthly ozone concentrations are less
than 9%. The simulations of 2-meter ozone concentrations from GCv12 show better seasonality when using the posterior
250   NO_x emissions than using the prior, as shown in Fig. 5. Simulations using the CEDS inventory show double maxima in April
and August, whereas surface measurements only show a single maximum in April. Assimilation of NASA NO_2
concentrations alleviates this difference and leads to the largest correlation with measured MDA8 and 24-hour average
ozone; simulations using the DOMINO posterior emissions have the largest correlation coefficient for daytime ozone. That
being said, the correlation coefficients are not notably different. Compared with CNEMC measurements in China,
255   simulations using the prior emissions have the most consistent seasonal variations and smallest NMSE. All simulations have
smaller seasonal variations than the measurements in daytime ozone.

3.3 Inter-annual variations

The three different versions of NO_x emissions have different regional trends from 2005 to 2016 as shown in Fig. 6. In China,
the NASA posterior NO_x emissions increased by 32% and the DOMINO posterior NO_x emissions increased by 32% from
260   2005 to 2011. From 2011 to 2016, they decreased by 20% (NASA) and 11% (DOMINO). This turning point reflects the

Atmospheric
Chemistry
and Physics
Discussions

Open Access

EGU

regulation of NO_x emissions in China since the "11th 5-year plan" in 2011. In India, both posterior NO_x emissions showed continuous increases (by 24% from the NASA posterior and 34% from the DOMINO posterior) from 2005 to 2016. The sources of NO_x emissions in India are mainly from thermal power and transportation and are expected to continue increasing in the near future under current regulations [Venkataraman et al., 2018]. In the US, NO_x emissions decreased by 24%

265 (NASA) and 19% (DOMINO) from 2005 to 2010 and then flattened from 2010 to 2016. This slowdown in the total top-down NO_x emissions was attributed to the growing contribution from industrial, areal, and off-road mobile sources as well as the slower than expected decreases in on-road diesel NO_x emissions by Jiang et al. [2018]. Silvern et al. [2019], however, argued that the slowdown was driven by the weaker decreases in background sources of NO_x, which has increasing contribution with the decrease of anthropogenic NO_x sources. In Mexico and Australia, the two posterior NO_x emissions

270 consistently increased by 6% (NASA) and 13% (DOMINO), and 11% (NASA) and 4% (DOMINO) from 2005 to 2016, respectively. The increase in Mexico is more obvious from 2010 to 2016 from the DOMINO posterior. This increase in Mexico is also not reflected in the bottom-up estimates from the EPA National Emissions Inventory. The trends of NO_x emissions in South America are different in the two posterior estimates after 2012, when the NASA posterior emissions started to decrease by 27% and the DOMINO posterior emissions started to increase by 11% up until 2016. Throughout the

275 period, posterior NO_x emissions have different trends in Western Europe and Africa where the NASA posterior showed decreases by 11% and 0.3%, and the DOMINO posterior showed increases by 5% and 11%, respectively.

The magnitudes of DOMINO posterior NO_x emissions are consistently larger than the NASA ones throughout the period. The 12-year averages of annual NO_x budgets from NASA posteriors are 37% (China), 53% (India), 43% (US), 50%

280 (Mexico), 45% (Australia), 58% (South America), 47% (Western Europe), and 46% (Africa) smaller than the DOMINO posterior.

We evaluate the trend of simulated surface NO_2 concentrations in the US with AQS measurements due to its availability throughout the study period (Fig. 7). From 2006 to 2016, the surface NO_2 concentrations show consistent decreases in the

285 AQS measurements (by 32%) and GC-adj simulations (by 26% using the NASA posterior, by 10% using the DOMINO posterior, and by 7% using the prior emissions). Since we use the same anthropogenic emissions throughout 2006-2016 in the prior simulations, the variations in the black line reflect changes from natural sources and the impact of meteorological factors (e.g., temperature, humidity, wind, etc.). Surface NO_2 simulations using the NASA posterior NO_x emissions also have the largest correlation coefficient when compared to the measurements ($R^2 = 0.93$ for the NASA posterior, $R^2 = 0.81$

290 for the DOMINO posterior, and $R^2 = 0.74$ for the prior). The more consistent trends and correlations in surface NO_2 simulations using the NASA posterior emissions are consistent with the larger decrease of NASA posterior NO_x emissions in the US (by 20%, or for comparison a decrease of 1% in the DOMINO posterior) from 2006 to 2016, as shown in Fig. 6.

The interannual variability of global simulations of 2-meter ozone sampled at the TOAR locations is similar between GC-adj

295 and GCv12. During the NH summer, simulations using the DOMINO posterior NO_x emissions have the most consistent trend in daytime and 24-hour average ozone in both models (see Table S1); GC-adj simulations using the NASA posterior emissions have the best consistency with the measured trend of MDA8 ozone. Detailed analyses of global ozone trends are in Sect. S3. At the regional scale, shown in Fig. 8, surface ozone measurements from TOAR mostly fall within the ranges of assimilation results. The interannual variations of simulated ozone over the whole region (black dotted lines) are generally

300 smaller than the ones at grid cells that include surface measurements (black solid lines). The number of years that ozone measurements are available in each grid cell is shown in Fig. S6. The overlap of solid black and green lines in Fig. 8 suggests that interannual variations of anthropogenic NO_x emissions from CEDS do not have a large impact on surface ozone simulations. The trends of simulated annual MDA8 ozone concentrations are correlated with impacts from meteorology and non-NO_x sources, leading to ozone changes of up to 4 ppbv (China), 5 ppbv (South Korea), 1ppbv (US), 2

305 ppbv (Mexico), 1 ppbv (South America), 1 ppbv (Australia), 1 ppbv (Western Europe), and 6 ppbv (Africa) from one year to the next. The trends of simulated MDA8 ozone are similar when using the NASA and the DOMINO posterior NO_x emissions as inputs. The simulated MDA8 ozone trends in grid cells that include measurements in the US and Australia are more consistent with the TOAR measurements than the other regions, with coefficients of determination (R^2) larger than 0.45. The larger differences in ozone between the prior and posterior emissions as well as variability between the two top-

310 down NO_x emissions in GCv12 suggest a larger responsiveness of the ozone chemistry to changes in NO_x. We do not expect simulated ozone trends to be completely consistent with the measurements in the TOAR database due to errors in the model's transport, chemical mechanism, and VOC emissions.

We further separate the ozone trends in grid cells that include measurements into changes caused by NO_x emissions as well

315 as meteorology and non-NO_x sources in Fig. 9. The ozone trends due to changes in meteorology and non-NO_x sources (green lines) are moderately correlated (R > 0.5) with measurements from TOAR in Australia, the US, South America, and India. The ozone trends due to changes in posterior NO_x emissions (red and blue lines) only have positive correlations with TOAR measurements in both GC-adj and GCv12 simulations in Africa and Australia. Ozone measurements in 2014 decreased compared to the 2006 level in China, the US, South America and Mexico. GC-adj simulations do not have big trends in these

320 regions, whereas GC-v12 simulations show increases in China, the US, and Mexico. Meteorological and non-NO_x sources lead to larger inter-annual variations in ozone simulations than those driven by NO_x emissions in South America, Australia, and Africa, where anthropogenic activities are much less than the other regions. These underscore the challenges of attributing observed variations in ozone to changes in NO_x emissions at regional scales.

4 Western US remote ozone

325 Assimilations of ozone precursor gases have the potential to improve remote ozone simulations, which can be used to provide boundary conditions for regional air quality models and to quantify and attribute sources of background ozone. We therefore focus specifically on remote regions in the US in this section to evaluate the vertical profile and surface concentrations of ozone simulations.

4.1 Evaluations with ozonesonde profiles

330 Field campaigns and routine observations of ozone concentrations along the west coast of the US have provided opportunities to understand regional and intercontinental influences on surface air quality [Cooper et al., 2015]. Evaluations with the IONS-2010 measurements in Fig. 10 show that the GCv12 simulations of ozone vertical profiles have negative biases (NMB between -8% and -32%) above all six sites. The standard deviations of ozonesonde and simulated profiles overlap with each other (see Fig. S7). The GC-adj simulations have positive biases at San Nicolas and Trinidad Head and

335 have smaller negative biases (NMB between -3% and -11%) at the remaining sites than the GCv12 simulations. The magnitudes of the NMSE and NMB of the GCv12 simulations at 700 – 900 hPa are also larger than those of the GC-adj simulations (see Fig. S8). The air masses at this altitude in the eastern Pacific are demonstrated to impact inland near surface ozone concentrations [Cooper et al., 2011; Lin et al., 2012; Yates et al., 2015]. The different biases in ozone simulations can be explained by the usage of different emission inventories (e.g., different biogenic emissions), different boundary layer

340 mixing scheme (non-local mixing [Lin and McElroy, 2010] in GCv12 and full mixing in GCadj), and differences in chemical mechanisms. For instance, inclusion of halogen chemistry and additional chlorine chemistry in GCv12 leads to 19% and 7% decreases of global tropospheric ozone burden [Sherwen et al., 2016a; Wang et al., 2019]. GCv12 simulations using the CEDS emissions have smaller NMSE and NMB than the simulations using the posterior NO_x emissions in all 6 sites in 2010. In comparison, the GC-adj simulations using the DOMINO posterior NO_x emissions have the smallest NMSE and NMB at

345 all sites except for San Nicolas and Trinidad Head, where the prior simulations have the smallest error and bias. Further evaluations with ozonesondes at Trinidad Head in 2016 are shown in Sect. S4.

4.2 Evaluations with TOAR surface ozone measurements at remote sites

To further evaluate the model performance under different geographical scenarios, we compare surface ozone simulations from GC-adj and GCv12 with observations from simple to complex environments. These include 1) Mauna Loa Observatory

350 and Mt Bachelor Observatory at night, which represent the lower free troposphere; 2) Mt. Bachelor Observatory, Lassen Volcanic National Park, Great Basin National Park, and Sequoia / Kings Canyon National Park at daytime, representing high elevation rural sites during well-mixed daytime conditions. The coefficients of determination (see Table S2) between the simulations and the measurements are larger than 0.6 for all daytime ozone comparisons except for Mt. Bachelor

355 Observatory. The correlation coefficients are smaller than 0.5 for all nighttime comparisons, reflecting the need to further improve simulations of nighttime chemistry and atmospheric processes.

In Fig. 11, the surface ozone concentrations from both GC-adj and GCv12 simulations have low biases compared to the surface measurements at remote sites. These low biases in the GCv12 simulations are consistent with its performances when evaluated with ozonesondes from IONS-2010 and with daytime surface ozone at the global scale. However, the low biases in 360 the GC-adj simulations are different from its high biases when compared with the global surface ozone concentrations and the ozone profiles at San Nicolas and Trinidad Head. This demonstrates the different biases in ozone simulations at rural and urban sites. Simulations using the DOMINO posterior emissions have the smallest NMSE and NMB at all remote sites except for the GCv12 simulations at Mauna Loa at night and Great Basin during the daytime.

5 Discussion and conclusions

365 We performed global inversions of NO_x emissions from 2005 to 2016 using two widely used OMI NO_2 retrievals from NASA (OMNO2 v3) and KNMI (DOMINO v2). The DOMINO posterior NO_x emissions have larger magnitude than the prior and the NASA posterior. Consequently, GC-adj simulations using the DOMINO posterior NO_x emissions have the smallest negative bias in surface NO_2 and the smallest positive bias in 2-meter ozone. The impact of NO_2 assimilations on improving estimates of the GCv12 surface ozone simulations depends upon the ozone metrics, suggesting inaccurate diurnal 370 variations in the surface ozone simulations. GEOS-Chem simulations using the DOMINO posterior emissions have the largest coefficients of determination for summertime daytime (R^2=0.81) and summertime 24-hour (R^2=0.96) ozone. Simulations using the NASA posterior emissions have the smallest bias and error for all ozone metrics and the largest correlation for summertime MDA8 ozone (R^2 = 0.88). Ozone simulations with GEOS-Chem v12.1.1 using the DOMINO posterior NO_x emissions lead to the most consistent seasonality in 24-hour average ozone (R^2 = 0.99) with TOAR 375 measurements, while the NASA posterior emissions lead to the best agreement in seasonal variations of MDA8 (R = 0.96) and daytime ozone (R = 0.98). The interannual variations of posterior NO_x emissions from the two products are similar in China, India, the US, Mexico and Australia, but different in South America, West Europe and Africa. Surface NO_2 simulations using the NASA posterior have the best agreement with measurements in the US. Daytime and 24-hour average ozone simulations using the DOMINO posterior also have the best trend (R = 0.72 and 0.88) in the Northern Hemisphere 380 summer. The GC-adj simulations using the NASA posterior NO_x emissions have the best trend in MDA8 ozone in NH summer.

Posterior NO_x emissions lead to improved simulations of ozone at several remote sites in the western US. The GC-adj simulations using the DOMINO posterior emissions have the smallest NMSE and NMB compared to ozonesonde 385 measurements during IONS-2010, except for the San Nicolas and Trinidad Head sites. At the remote surface sites evaluated

12

in this study, surface ozone simulations using the DOMINO posterior emissions have the best performance except for GCv12 simulations at Mauna Loa at night and Great Basin during the daytime. The reduced negative biases in daytime surface ozone simulations using the DOMINO posterior emissions at these remote sites and at most IONS-2010 sites are consistent with the increases of daytime remote ozone in the western US through NO_2 and ozone data assimilation in Huang

390 et al. [2015]. Simulations using the DOMINO posterior emissions are demonstrated to provide more precise magnitudes at these remote sites and can potentially be used as boundary conditions for regional air quality models for further air pollution and health studies.

The remaining differences between simulated and measured ozone can be explained by the roles of VOCs, errors in satellite

395 retrievals, and uncertainties in the chemical and physical processes in the model simulations. In addition to NO_x, emissions of other ozone precursors also impact the accuracy of ozone simulations. For instance, inversion of isoprene emissions over the southeast US decreases surface ozone simulations by 1-3 ppbv [Kaiser et al., 2018]. Inversion of non-methane VOC emissions changes surface afternoon ozone simulations by up to 10 ppbv in China [Cao et al., 2018]. Both OMI NO_2 retrievals employed in this study use NO_2 vertical shape factors from coarse resolution simulations, and therefore are biased

400 low compared to in-situ measurements [Goldberg et al., 2017]. These retrievals also have not explicitly accounted for the aerosol optical effects, which are demonstrated to degrade the accuracy of NO_2 column concentrations [Chimot et al., 2016; Liu et al., 2019; Cooper et al., 2019]. The differences in the magnitude of ozone concentrations from GC-adj and GCv12 reflect the impact of other species emissions and chemical mechanisms on the bias of ozone simulations. Previous studies also show that global simulations at coarse resolution are not able to capture the observed persistence of chemical plumes in

405 the free troposphere on intercontinental scales, therefore leading to underestimates of remote ozone concentrations [Hudman et al., 2004; Zhuang et al., 2018].

Although biases, errors, seasonalities and inter-annual variations of ozone simulations have been improved in several cases through constraints on NO_x emissions, there are still large discrepancies in the vertical profile and diurnal variations between

410 ozone simulations and measurements. For instance, the different performances of each set of NO_x emissions on the simulations of different ozone metrics reflect errors in the ozone diurnal simulations. The differences in ozone vertical profiles suggest errors in vertical transport in the model. These discrepancies could not be improved by adjusting only surface NO_x emissions using observations at one time of the day, as performed in this study. Future geostationary satellite observations will provide opportunities to update NO_x emissions at every hour. Separately constraining NO_x emissions from

415 surface (e.g., anthropogenic sources) and upper atmosphere (e.g., lightning sources [Pickering et al., 2016]) and implementing these posterior NO_x emissions at their corresponding vertical levels can potentially improve the vertical profile of ozone simulations.

Atmospheric
Chemistry
and Physics
Discussions

Author contribution

Z.Q., D.K.H., O.R.C, and J.L.N. designed the research; Z. Q. performed the research and prepared the paper with help from all authors.

References

Bell, N., L. Hsu, D. J. Jacob, M. G. Schultz, D. R. Blake, J. H. Butler, D. B. King, J. M. Lobert, and E. Maier-Reimer: Methyl iodide: Atmospheric budget and use as a tracer of marine convection in global models, J. Geophys. Res. Atmos., 107(D17), ACH 8–1–ACH 8–12, doi:10.1029/2001JD001151, 2002.

14

Boersma, K. F. et al.: An improved tropospheric NO2 column retrieval algorithm for the Ozone Monitoring Instrument, Atmos. Meas. Tech., 4(9), 1905–1928, doi:10.5194/amt-4-1905-2011, 2011.

Boersma, K. F. et al.: Improving algorithms and uncertainty estimates for satellite NO2 retrievals: results from the quality assurance for the essential climate variables (QA4ECV) project, Atmos. Meas. Tech., 11(12), 6651–6678, 2018.

455   Canty, T. P., L. Hembeck, T. P. Vinciguerra, D. C. Anderson, D. L. Goldberg, S. F. Carpenter, D. J. Allen, C. P. Loughner, R. J. Salawitch, and R. R. Dickerson: Ozone and NOx chemistry in the eastern US: evaluation of CMAQ/CB05 with satellite (OMI) data, Atmos. Chem. Phys., 15(19), 10965–10982, doi:10.5194/acp-15-10965-2015, 2015.

Cao, H. et al.: Adjoint inversion of Chinese non-methane volatile organic compound emissions using space-based observations of formaldehyde and glyoxal, Atmos. Chem. Phys., 18(20), 15017–15046, 2018.

460   Chan Miller, C. et al.: Glyoxal yield from isoprene oxidation and relation to formaldehyde: chemical mechanism, constraints from SENEX aircraft observations, and interpretation of OMI satellite data, Atmos. Chem. Phys., 17(14), 8725–8738, doi:10.5194/acp-17-8725-2017, 2017.

Chimot, J., T. Vlemmix, J. P. Veefkind, J. F. de Haan, and P. F. Levelt: Impact of aerosols on the OMI tropospheric NO2 retrievals over industrialized regions: how accurate is the aerosol correction of cloud-free scenes via a simple cloud
465   model? Atmos. Meas. Tech., 9(2), 359–382, doi:10.5194/amt-9-359-2016, 2016.

Cooper, M. J., R. V. Martin, M. S. Hammer, and C. A. McLinden: An Observation-Based Correction for Aerosol Effects on Nitrogen Dioxide Column Retrievals Using the Absorbing Aerosol Index, Geophys. Res. Lett., 46(14), 8442–8452, doi:10.1029/2019GL083673, 2019.

Cooper, O. R. et al.: Evidence for a recurring eastern North America upper tropospheric ozone maximum during summer, J.
470   Geophys. Res. Atmos., 112(D23), doi:10.1029/2007JD008710, 2007.

Cooper, O. R. et al.: Measurement of western U.S. baseline ozone from the surface to the tropopause and assessment of downwind impact regions, J. Geophys. Res. Atmos., 116(D21), doi:10.1029/2011JD016095, 2011.

Cooper, O. R., A. O. Langford, D. D. Parrish, and D. W. Fahey: Challenges of a lowered U.S. ozone standard, Science, 348(6239), 1096–1097, doi:10.1126/science.aaa5748, 2015.

475   Crutzen, P.: A discussion of the chemistry of some minor constituents in the stratosphere and troposphere, Pure App. Geophys., 106(1), 1385–1399, 1973.

Atmospheric
Chemistry
and Physics
Discussions

Derwent, R. G., M. E. Jenkin, and S. M. Saunders: Photochemical ozone creation potentials for a large number of reactive hydrocarbons under European conditions, Atmos. Environ., 30(2), 181–199, 1996.

Duncan, B. N., L. N. Lamsal, A. M. Thompson, Y. Yoshida, Z. Lu, D. G. Streets, M. M. Hurwitz, and K. E. Pickering: A
480   space-based, high-resolution view of notable changes in urban NOx pollution around the world (2005–2014), J. Geophys. Res. Atmos., 121(2), 976–996, doi:10.1002/2015JD024121, 2016.

Dunlea, E. J. et al.: Evaluation of nitrogen dioxide chemiluminescence monitors in a polluted urban environment, Atmos. Chem. Phys., 7(10), 2691–2704, 2007.

Eastham, S. D., D. K. Weisenstein, and S. R. H. Barrett: Development and evaluation of the unified tropospheric–
485   stratospheric chemistry extension (UCX) for the global chemistry-transport model GEOS-Chem, Atmos. Environ., 89, 52–63, 2014.

Fiore, A. M., J. T. Oberman, M. Y. Lin, L. Zhang, O. E. Clifton, D. J. Jacob, V. Naik, L. W. Horowitz, J. P. Pinto, and G. P. Milly: Estimating North American background ozone in U.S. surface air with two independent global models: Variability, uncertainties, and recommendations, Atmos. Environ., 96, 284–300, 2014.

490   Fiore, A. M., V. Naik, and E. M. Leibensperger: Air Quality and Climate Connections, J. Air Waste Manage., 65(6), 645–685, doi:10.1080/10962247.2015.1040526, 2015.

Fisher, J. A. et al.: Organic nitrate chemistry and its implications for nitrogen budgets in an isoprene- and monoterpene-rich atmosphere: constraints from aircraft (SEAC4RS) and ground-based (SOAS) observations in the Southeast US, Atmos. Chem. Phys., 16(9), 5969–5991, doi:10.5194/acp-16-5969-2016, 2016.

495   Fleming, Z. L. et al.: Tropospheric Ozone Assessment Report: Present-day ozone distribution and trends relevant to human health, Elem Sci Anth, 6(1), 12, doi:doi.org/10.1525/elementa.273, 2018.

Fowler, D. et al.: Atmospheric Composition Change: ecosystems-Atmosfere Interactions, Atmos. Environ., 43, 5193–5267, doi:10.1016/j.atmosenv.2009.07.068, 2009.

Gaudel, A. et al.: Tropospheric Ozone Assessment Report: Present-day distribution and trends of tropospheric ozone relevant
500   to climate and global atmospheric chemistry model evaluation, Elem. Sci. Anth., 6(1), 39, doi:10.1525/elementa.291, 2018.

Goldberg, D. L., L. N. Lamsal, C. P. Loughner, W. H. Swartz, Z. Lu, and D. G. Streets: A high-resolution and observationally constrained OMI NO2 satellite retrieval, Atmos. Chem. Phys., 17(18), 11403–11421, doi:10.5194/acp-

17-11403-2017, 2017.

505 Goldstein, A. H., D. B. Millet, M. McKay, L. Jaegle, L. Horowitz, O. Cooper, R. Hudman, D. J. Jacob, S. Oltmans, and A. Clarke: Impact of Asian emissions on observations at Trinidad Head, California, during ITCT 2K2, J. Geophys. Res. Atmos., 109(D23), doi:10.1029/2003JD004406, 2004.

Henze, D. K., A. Hakami, and J. H. Seinfeld: Development of the adjoint of GEOS-Chem, Atmos. Chem. Phys., 7(9), 2413–2433, doi:10.5194/acp-7-2413-2007, 2007.

510 Henze, D. K., J. H. Seinfeld, and D. T. Shindell: Inverse modeling and mapping US air quality influences of inorganic PM2.5 precursor emissions using the adjoint of GEOS-Chem, Atmos. Chem. Phys., 9(16), 5877–5903, 2009.

Herman, J., N. Abuhassan, J. Kim, M. Dubey, M. Raponi, and M. Tzortziou: Underestimation of Column NO2 Amounts from the OMI Satellite Compared to Diurnally Varying Ground-Based Retrievals from Multiple Pandora Spectrometer Instruments, AMTD, 2019, 1–35, doi:doi.org/10.5194/amt-2019-123, 2019.

515 Hoesly, R. M. et al.: Historical (1750–2014) anthropogenic emissions of reactive gases and aerosols from the Community Emissions Data System (CEDS), Geosci. Model Dev., 11(1), 369–408, doi:10.5194/gmd-11-369-2018, 2018.

Hsu, J., and M. J. Prather: Stratospheric variability and tropospheric ozone, J. Geophys. Res. Atmos., 114(D6), doi:10.1029/2008JD010942, 2009.

Huang, M., K. W. Bowman, G. R. Carmichael, M. Lee, T. Chai, S. N. Spak, D. K. Henze, A. S. Darmenov, and A. M. da
520 Silva: Improved western U.S. background ozone estimates via constraining nonlocal and local source contributions using Aura TES and OMI observations, J. Geophys. Res. Atmos., 120(8), 3572–3592, doi:10.1002/2014JD022993, 2015.

Hudman, R. C. et al.: Ozone production in transpacific Asian pollution plumes and implications for ozone air quality in California, J. Geophys. Res. Atmos., 109(D23), doi:10.1029/2004JD004974, 2004.

525 Jaffe, D. A., O. R. Cooper, A. M. Fiore, B. H. Henderson, G. S. Tonneson, A. G. Russell, D. K. Henze, A. O. Langford, M. Lin, and T. Moore: Scientific assessment of background ozone over the U.S.: Implications for air quality management, Elem Sci Anth, 6(1), 56, doi:http://doi.org/10.1525/elementa.309, 2018.

Janssens-Maenhout, G. et al.: HTAP_v2.2: a mosaic of regional and global emission grid maps for 2008 and 2010 to study hemispheric transport of air pollution, Atmos. Chem. Phys., 15(19), 11411–11432, doi:10.5194/acp-15-11411-2015,
530 2015.

Jiang, Z. et al.: Unexpected slowdown of US pollutant emission reduction in the past decade, Proc. Natl. Acad. Sci., 115(20), 5099–5104, doi:10.1073/pnas.1801191115, 2018.

Johnson, B. J., S. J. Oltmans, H. Vömel, H. G. J. Smit, T. Deshler, and C. Kröger: Electrochemical concentration cell (ECC) ozonesonde pump efficiency measurements and tests on the sensitivity to ozone of buffered and unbuffered ECC sensor cathode solutions, J. Geophys. Res. Atmos., 107(D19), ACH 8–1–ACH 8–18, doi:10.1029/2001JD000557, 2002.

Kaiser, J. et al.: High-resolution inversion of OMI formaldehyde columns to quantify isoprene emission on ecosystem-relevant scales: application to the southeast US, Atmos. Chem. Phys., 18(8), 5483–5497, 2018.

Keller, C. A., M. S. Long, R. M. Yantosca, A. M. Da Silva, S. Pawson, and D. J. Jacob: HEMCO v1.0: a versatile, ESMF-compliant component for calculating emissions in atmospheric models, Geosci. Model Dev., 7(4), 1409–1417, doi:10.5194/gmd-7-1409-2014, 2014.

Krotkov, N. A. et al.: Aura OMI observations of regional SO_2 and NO_2 pollution changes from 2005 to 2015, Atmos. Chem. Phys., 16, 4605–4629, doi:10.5194/acp-16-4605-2016, 2016.

Krotkov, N. A., L. N. Lamsal, E. A. Celarier, W. H. Swartz, S. V. Marchenko, E. J. Bucsela, K. L. Chan, M. Wenig, and M. Zara: The version 3 OMI NO2 standard product, Atmos. Meas. Tech., 10(9), 3133–3149, doi:10.5194/amt-10-3133-2017, 2017.

Lamsal, L. N., R. V. Martin, A. van Donkelaar, M. Steinbacher, E. A. Celarier, E. Bucsela, E. J. Dunlea, and J. P. Pinto: Ground-level nitrogen dioxide concentrations inferred from the satellite-borne Ozone Monitoring Instrument, J. Geophys. Res. Atmos., doi:10.1029/2007JD009235, 2008.

Lin, J. and M. B. McElroy: Impacts of boundary layer mixing on pollutant vertical profiles in the lower troposphere: Implications to satellite remote sensing, Atmos. Environ., 44, 1726-1739, doi:10.1016/j.atmosenv.2010.02.009, 2010.

Lin, M. et al.: Transport of Asian ozone pollution into surface air over the western United States in spring, J. Geophys. Res. Atmos., 117, D00V07, doi:10.1029/2011JD016961, 2012.

Lin, M., L. W. Horowitz, R. Payton, A. M. Fiore, and G. Tonnesen: US surface ozone trends and extremes from 1980 to 2014: quantifying the roles of rising Asian emissions, domestic controls, wildfires, and climate, Atmos. Chem. Phys., 17(4), 2943–2970, doi:10.5194/acp-17-2943-2017, 2017.

Liu, F., Q. Zhang, R. J. van der A, B. Zheng, D. Tong, L. Yan, Y. Zheng, and K. He: Recent reduction in NO x emissions over China: synthesis of satellite observations and emission inventories, Environ. Res. Lett., 11(11), 114002,

doi:10.1088/1748-9326/11/11/114002, 2016.

Liu, M. et al.: Improved aerosol correction for OMI tropospheric NO2 retrieval over East Asia: constraint from CALIOP
560   aerosol vertical profile, Atmos. Meas. Tech., 12(1), 1–21, 2019.

Malley, C. S., D. K. Henze, J. C. I. Kuylenstierna, H. W. Vallack, Y. Davila, S. C. Anenberg, M. C. Turner, and M. R.
Ashmore: Updated global estimates of respiratory mortality in adults $\geq$ 30 years of age attributable to long-term ozone
exposure, Environ. Health Perspect., 125(8), 087021, doi:10.1289/EHP1390, 2017.

Marais, E. A. et al.: Aqueous-phase mechanism for secondary organic aerosol formation from isoprene: application to the
565   southeast United States and co-benefit of SO2 emission controls, Atmos. Chem. Phys., 16(3), 1603–1618, 2016.

Miyazaki, K., H. Eskes, K. Sudo, K. F. Boersma, K. Bowman, and Y. Kanaya: Decadal changes in global surface NO_X
emissions from multi-constituent satellite data assimilation, Atmos. Chem. Phys., 17(2), 807–837, doi:10.5194/acp-17-
807-2017, 2017.

Monks, P. S. et al.: Tropospheric ozone and its precursors from the urban to the global scale from air quality to short-lived
570   climate forcer, Atmos. Chem. Phys., 15(15), 8889–8973, doi:10.5194/acp-15-8889-2015, 2015.

National Research Council (NRC): Rethinking the ozone problem in urban and regional air pollution, National Academy
Press, Washington D.C, 1991.

Parrella, J. P. et al.: Tropospheric bromine chemistry: implications for present and pre-industrial ozone and mercury, Atmos.
Chem. Phys., 12(15), 6723–6740, doi:10.5194/acp-12-6723-2012, 2012.

575 Pickering, K. E., E. Bucsela, D. Allen, A. Ring, R. Holzworth, and N. Krotkov: Estimates of lightning NOx production based
on OMI NO2 observations over the Gulf of Mexico, J. Geophys. Res. Atmos., 121(14), 8668–8691,
doi:10.1002/2015JD024179, 2016.

Qu, Z., D. K. Henze, S. L. Capps, Y. Wang, X. Xu, J. Wang, and M. Keller: Monthly top-down NOx emissions for China
(2005–2012): A hybrid inversion method and trend analysis, J. Geophys. Res. Atmos., 122(8), 4600–4625, 2017.

580 Qu, Z., D. K. Henze, N. Theys, J. Wang, and W. Wang: Hybrid Mass Balance/4D-Var Joint Inversion of NOx and SO2
Emissions in East Asia, J. Geophys. Res. Atmos., 124(14), 8203–8224, doi:10.1029/2018JD030240, 2019.

Ryerson, T. B. et al.: The 2010 California Research at the Nexus of Air Quality and Climate Change (CalNex) field study, J.
Geophys. Res. Atmos., 118, 5830-5866, doi:10.1002/jgrd.50331, 2013.

585   Schmidt, J. A. et al.: Modeling the observed tropospheric BrO background: Importance of multiphase chemistry and implications for ozone, OH, and mercury, J. Geophys. Res. Atmos., 121(19), 11–819–11–835, doi:10.1002/2015JD024229, 2016.

Schultz, M. G. et al.: Tropospheric Ozone Assessment Report: Database and metrics data of global surface ozone observations, Elem. Sci. Anth., 5, 58, doi:10.1525/elementa.244, 2017.

Sherwen, T. et al.: Global impacts of tropospheric halogens (Cl, Br, I) on oxidants and composition in GEOS-Chem, Atmos.
590   Chem. Phys., 16(18), 12239–12271, doi:10.5194/acp-16-12239-2016, 2016a.

Sherwen, T. et al.: Iodine's impact on tropospheric oxidants: a global model study in GEOS-Chem, Atmos. Chem. Phys., 16(2), 1161–1186, doi:10.5194/acp-16-1161-2016, 2016b.

Sherwen, T., M. J. Evans, L. J. Carpenter, J. A. Schmidt, and L. J. Mickley: Halogen chemistry reduces tropospheric O3 radiative forcing, Atmos. Chem. Phys., 17(2), 1557–1569, doi:10.5194/acp-17-1557-2017, 2017.

595   Silvern, R. F. et al.: Using satellite observations of tropospheric NO2 columns to infer long-term trends in US NOx emissions: the importance of accounting for the free tropospheric NO2 background, Atmos. Chem. Phys., 19(13), 8863–8878, 2019.

Simon, H., A. Reff, B. Wells, J. Xing, and N. Frank: Ozone Trends Across the United States over a Period of Decreasing NOx and VOC Emissions, Environ. Sci. Technol., 49(1), 186–195, doi:10.1021/es504514z, 2015.

600   Smit, H. G. J. et al.: Assessment of the performance of ECC-ozonesondes under quasi-flight conditions in the environmental simulation chamber: Insights from the Juelich Ozone Sonde Intercomparison Experiment (JOSIE), J. Geophys. Res. Atmos., 112(D19), doi:10.1029/2006JD007308, 2007.

Steinbacher, M., C. Zellweger, B. Schwarzenbach, S. Bugmann, B. Buchmann, C. Ordóñez, A. S. H. Prevot, and C. Hueglin: Nitrogen oxide measurements at rural sites in Switzerland: Bias of conventional measurement techniques, J. Geophys.
605   Res. Atmos., 112(D11), doi:10.1029/2006JD007971, 2007.

Stevenson, D. S. et al.: Multimodel ensemble simulations of present-day and near-future tropospheric ozone, J. Geophys. Res. Atmos., 111(D8), doi:10.1029/2005JD006338, 2006.

Stohl, A. et al.: Stratosphere-troposphere exchange: A review, and what we have learned from STACCATO, J. Geophys. Res. Atmos., 108(D12), doi:10.1029/2002JD002490, 2003.

610 Thompson, A. M. et al.: Intercontinental Chemical Transport Experiment Ozonesonde Network Study (IONS) 2004: 1. Summertime upper troposphere/lower stratosphere ozone over northeastern North America, J. Geophys. Res. Atmos., 112(D12), doi:10.1029/2006JD007441, 2007.

Thompson, A. M., J. E. Yorks, S. K. Miller, J. C. Witte, K. M. Dougherty, G. A. Morris, D. Baumgardner, L. Ladino, and B. Rappenglück: Tropospheric ozone sources and wave activity over Mexico City and Houston during
615 MILAGRO/Intercontinental Transport Experiment (INTEX-B) Ozonesonde Network Study, 2006 (IONS-06), Atmos. Chem. Phys., 8(17), 5113–5125, 2008.

Travis, K. R. et al.: Why do models overestimate surface ozone in the Southeast United States? Atmos. Chem. Phys., 16(21), 13561–13577, 2016.

Turner, M. C. et al.: Long-Term Ozone Exposure and Mortality in a Large Prospective Study, Am. J. Respir. Crit. Care
620 Med., 193(10), 1134–1142, doi:10.1164/rccm.201508-1633OC, 2016.

United Nations Economic Commission For Europe (UNECE): Hemispheric Transport of Air Pollution 2010, 2010.

Valin, L. C., A. R. Russell, R. C. Hudman, and R. C. Cohen: Effects of model resolution on the interpretation of satellite NO_2 observations, Atmos. Chem. Phys., 11(22), 11647–11655, 2011.

Venkataraman, C. et al.: Source influence on emission pathways and ambient PM2.5 pollution over India (2015–2050),
625 Atmos. Chem. Phys., 18(11), 8017–8039, doi:10.5194/acp-18-8017-2018, 2018.

Venkataraman, C., G. Habib, D. Kadamba, M. Shrivastava, J. F. Leon, B. Crouzille, O. Boucher, and D. G. Streets: Emissions from open biomass burning in India: Integrating the inventory approach with high-resolution Moderate Resolution Imaging Spectroradiometer (MODIS) active-fire and land cover data, Global Biogeochem. Cy., 20(2), doi:10.1029/2005GB002547, 2006.

630 Verstraeten, W. W., J. L. Neu, J. E. Williams, K. W. Bowman, J. R. Worden, and K. F. Boersma: Rapid increases in tropospheric ozone production and export from China, Nat. Geosci., 8(9), 690–695, doi:10.1038/ngeo2493, 2015.

Wang, X. et al.: The role of chlorine in global tropospheric chemistry, Atmos. Chem. Phys., 19(6), 3981–4003, doi:10.5194/acp-19-3981-2019, 2019.

Yates, E. L., L. T. Iraci, D. Austerberry, R. B. Pierce, M. C. Roby, J. M. Tadić, M. Loewenstein, and W. Gore:
635 Characterizing the impacts of vertical transport and photochemical ozone production on an exceedance area, Atmos. Environ., 109, 342–350, doi:10.1016/j.atmosenv.2014.09.002, 2015.

Young, P. J. et al.: Pre-industrial to end 21st century projections of tropospheric ozone from the Atmospheric Chemistry and Climate Model Intercomparison Project (ACCMIP), Atmos. Chem. Phys., 13(4), 2063–2090, doi:10.5194/acp-13-2063-2013, 2013.

640 Zhang, L., D. J. Jacob, M. Kopacz, D. K. Henze, K. Singh, and D. A. Jaffe: Intercontinental source attribution of ozone pollution at western U.S. sites using an adjoint method, Geophys. Res. Lett., 36(11), doi:10.1029/2009GL037950, 2009.

Zhang, L., D. J. Jacob, X. Yue, N. V. Downey, D. A. Wood, and D. Blewitt: Sources contributing to background surface ozone in the US Intermountain West, Atmos. Chem. Phys., 14(11), 5295–5309, doi:doi.org/10.5194/acp-14-5295-2014, 2014.

645 Zhang, Y., O. R. Cooper, A. Gaudel, A. M. Thompson, P. Nédélec, S.-Y. Ogino, and J. J. West: Tropospheric ozone change from 1980 to 2010 dominated by equatorward redistribution of emissions, Nat. Geosci., 9, 875–879, doi:10.1038/NGEO2827, 2016.

Zheng, F., T. Yu, T. Cheng, X. Gu, and H. Guo: Intercomparison of tropospheric nitrogen dioxide retrieved from Ozone Monitoring Instrument over China, Atmos. Pollut. Res., 5(4), 686–695, 2014.

650 Zhuang, J., D. J. Jacob, and S. D. Eastham: The importance of vertical resolution in the free troposphere for modeling intercontinental plumes, Atmos. Chem. Phys., 18(8), 6039–6055, doi:10.5194/acp-18-6039-2018, 2018.

Zoogman, P. et al.: Tropospheric emissions: Monitoring of pollution (TEMPO), J. Quant. Spectrosc. Ra. , 186, 17-39, doi:10.1016/j.jqrst.2016.05.008, 2017.

655 **Table 1. Total NO$_x$ emission (anthropogenic + natural) budgets in 2010 [Tg N yr^{-1}]**

	Bottom-up	NASA posterior	DOMINO posterior	QA4ECV posterior
Global	52.20	51.86	61.36	57.97
China	9.85	9.57	11.94	10.30
US	5.69	5.63	7.45	6.78
India	4.03	4.04	5.16	4.74
Western Europe	3.13	3.09	4.33	3.57
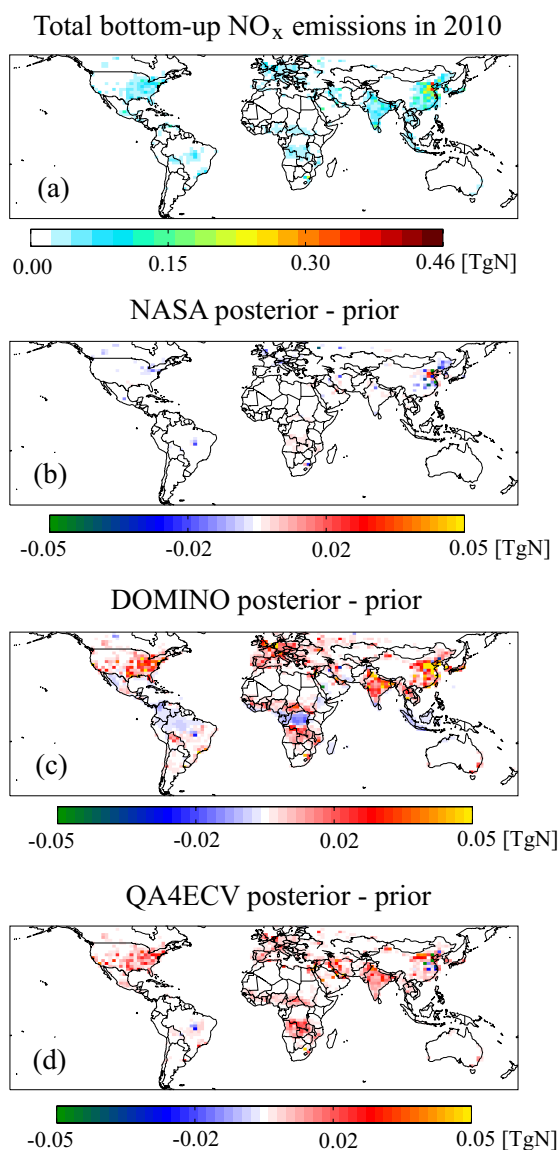
Figure 1. (a) Global total NO$_x$ emissions from the bottom-up inventory and the differences between 4D-Var posterior and bottom-
660 up estimates constrained by (b) NASA standard product v3, (c) DOMINO product v2, and (d) QA4ECV product in 2010.

24
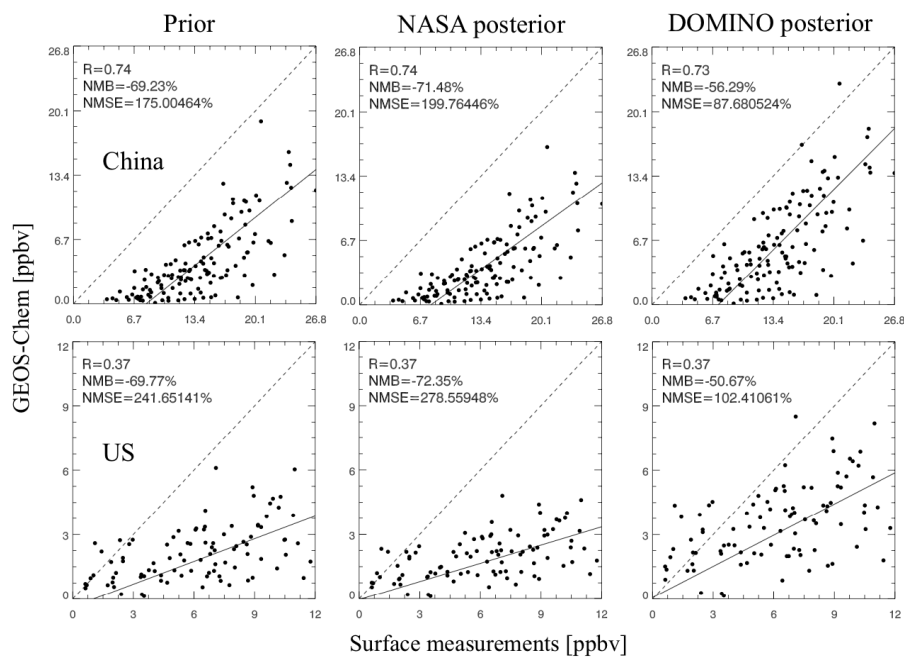
Figure 2. Evaluation of annual mean surface NO$_2$ mixing ratios with measurements in China (top) and the US (bottom) in 2015.

665

25
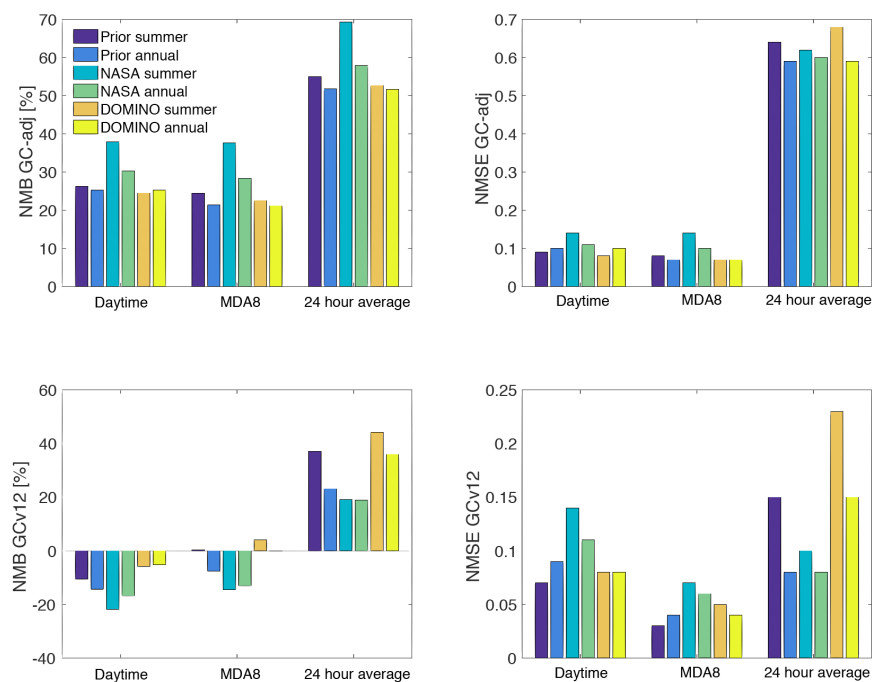
Figure 3. NMB and NMSE of annual mean and NH summertime surface ozone concentrations when comparing all measurements from TOAR in 2010 with GC-adj (top) and GCv12 (bottom) simulations. The simulations are input with three sets of NO$_x$ emissions: CEDS bottom-up inventory (HTAP for GC-adj and CEDS for GCv12), posterior emissions constrained by the NASA product, and posterior emissions constrained by the DOMINO product.
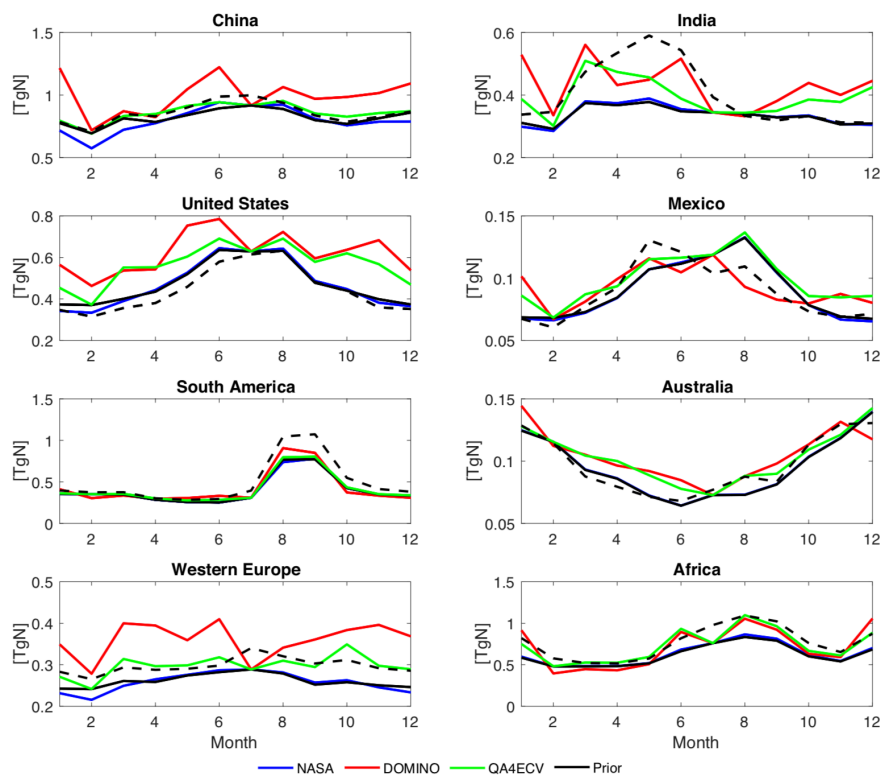
Figure 4. Seasonal variations of total 4D-Var posterior NO$_x$ emissions in 2010. The black lines are prior emissions from bottom-up inventories (solid lines are from GC-adj, dashed lines are from GCv12). The blue lines are the emissions constrained by OMI NO$_2$ NASA product. The red lines are emissions constrained by OMI NO$_2$ DOMINO product. The green lines are emissions constrained by OMI NO$_2$ QA4ECV product.
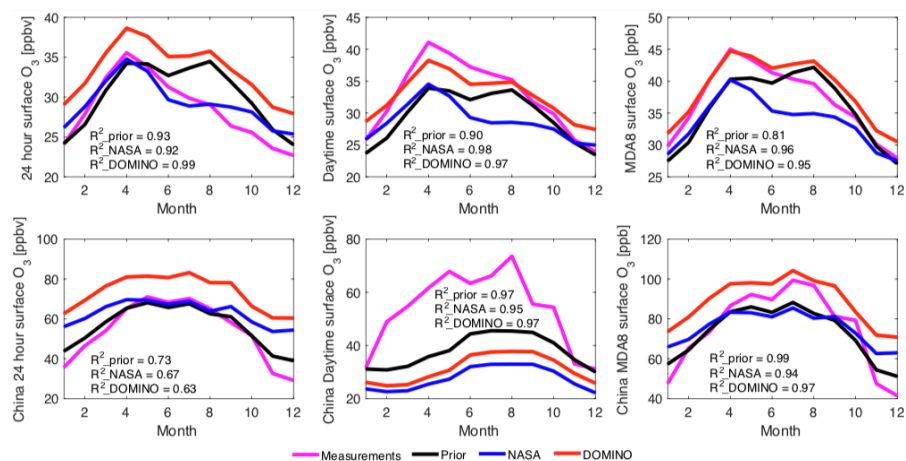
Figure 5. Seasonality of surface ozone concentration at 2 meters in 2010 compared with TOAR (top) and in 2015 compared with CNEMC (bottom). Surface measurements are shown in magenta lines. Simulations are performed using GCv12 with NO$_x$ emissions from CEDS (black line), NASA posterior (blue line) and DOMINO posterior (red line).
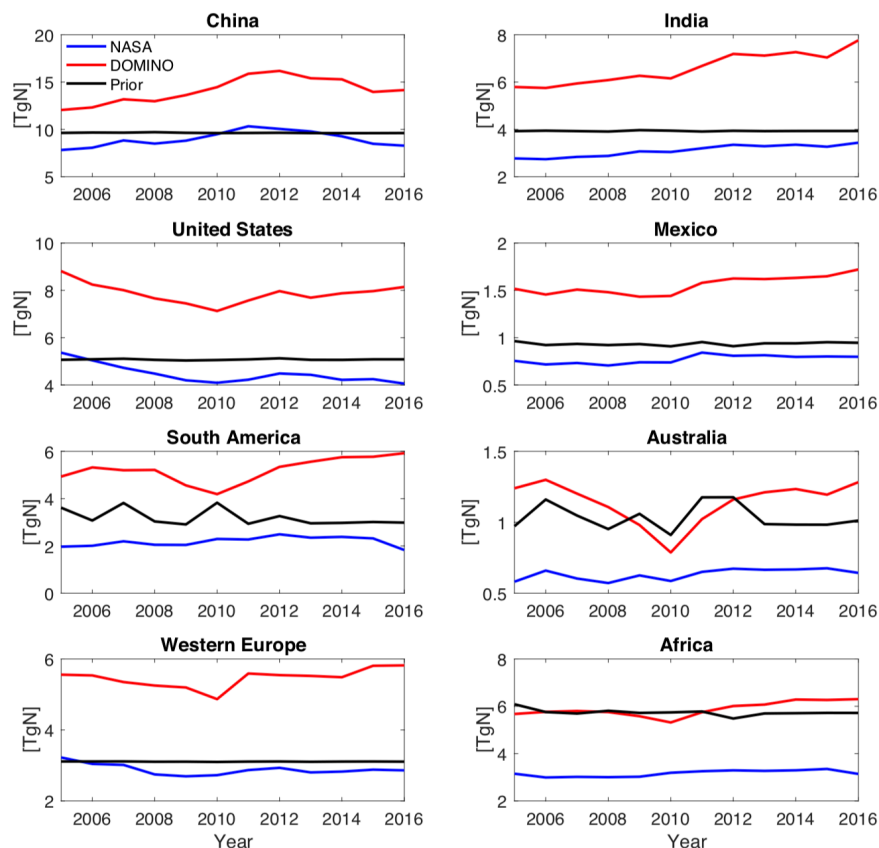
685

28

Figure 6. Annual total posterior NO$_x$ emissions from 2005 to 2016. The black lines show prior total NO$_x$ emissions from bottom-up inventories, which use HTAP anthropogenic emissions in 2010 for all years. The blue lines represent the emissions constrained by the OMI NO$_2$ NASA product. The red lines represent emissions constrained by the OMI NO$_2$ DOMINO product.
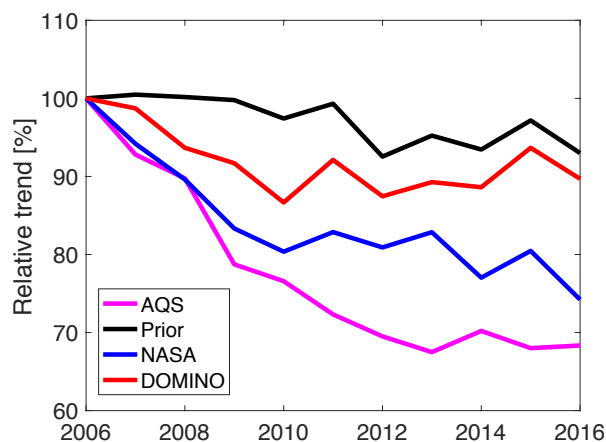
690

29

Figure 7. The trend of annual mean surface NO$_2$ concentrations over the US from 2006 to 2016, expressed as a percent of the 2006 values. Surface measurements are from EPA AQS sites (magenta line). GEOS-Chem simulations are performed using prior emissions (black line) with constant anthropogenic emissions throughout the years, posterior NO$_x$ emissions constrained by NASA product (blue line), and posterior NO$_x$ emissions constrained by DOMINO product (red line).

695

Atmospheric
Chemistry
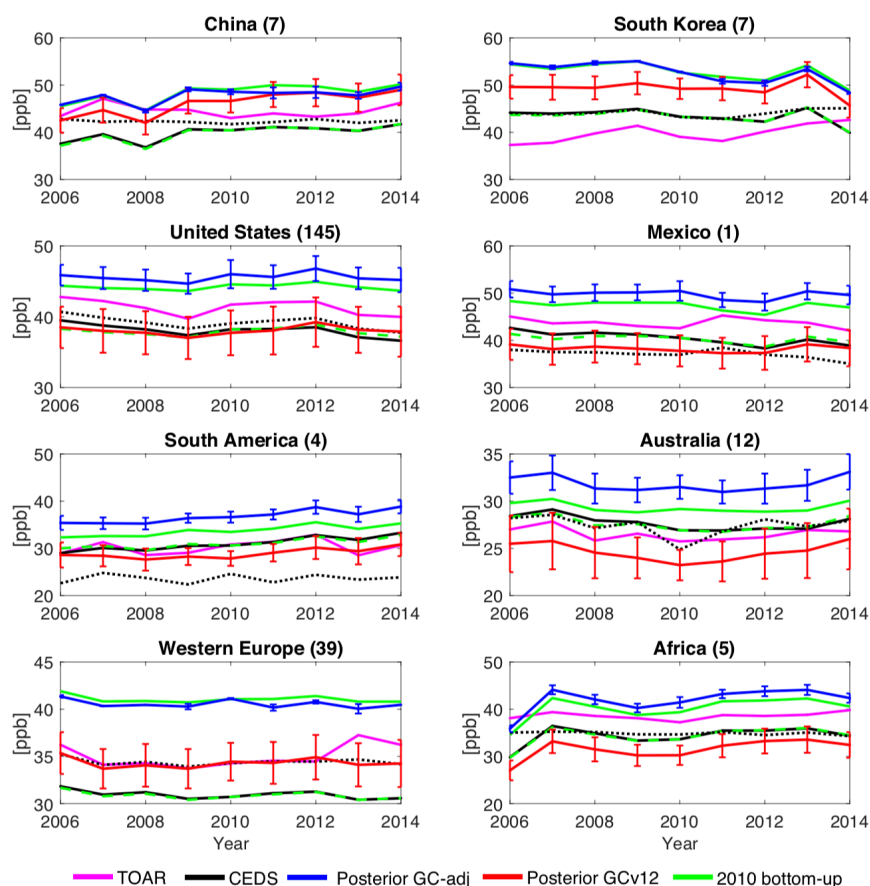and Physics
Discussions
Open Access
EGU

Figure 8. The trends of regional mean annual MDA8 ozone concentrations from 2006 to 2014. Surface measurements are from the TOAR database (magenta line). Only sites that have continuous measurements throughout the 9 years are included. The numbers
700 **in the parenthesis are the number of 2° × 2.5° grid cells that include monitoring sites in each region. The black dotted lines show national mean of surface ozone from GCv12 simulations using the CEDS inventory. The other lines are simulations from GC-adj and GCv12 averaged over the 2° × 2.5° grid cells that include monitoring sites. Black lines show ozone simulations using the bottom-up NO$_x$ emissions from CEDS in each corresponding year. Green lines show ozone simulations using 2010 bottom-up NO$_x$ emissions for all years (HTAP 2010 for GC-adj shown in solid lines, CEDS 2010 for GCv12 shown in dashed lines). The vertical**
705 **bars represent the spread of simulated surface ozone concentrations using the NASA and the DOMINO posterior NO$_x$ emissions.**

Atmospheric
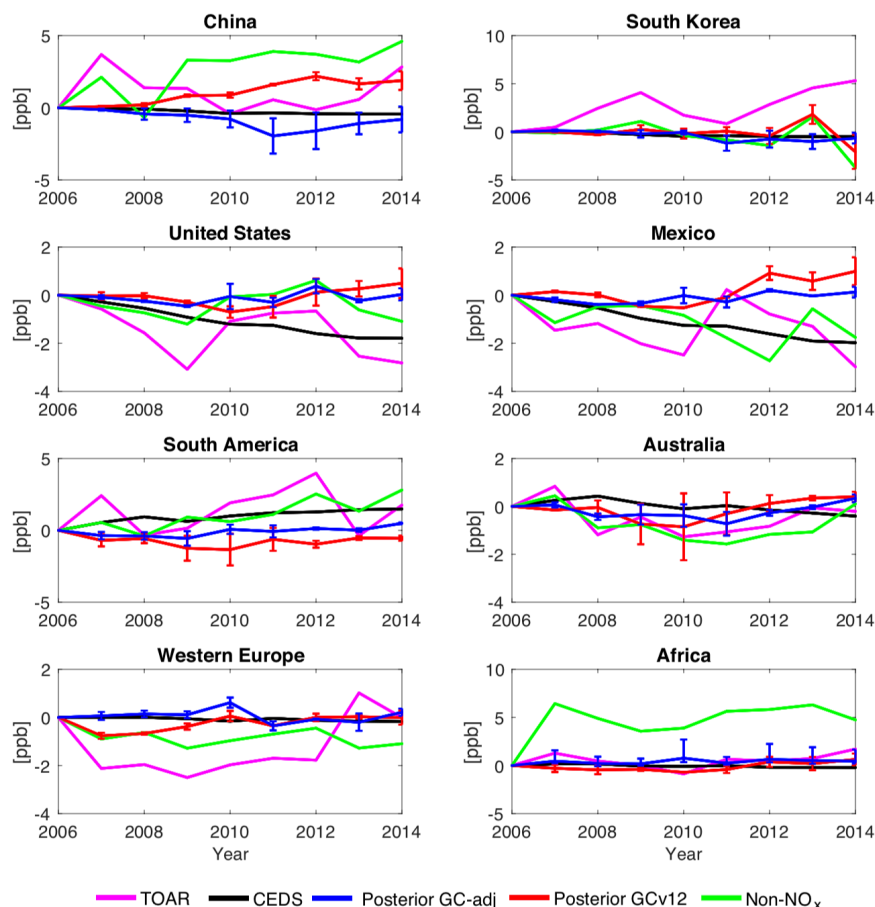Chemistry
and Physics
Discussions
Open Access
EGU

Figure 9. Changes of regional mean annual MDA8 ozone concentrations compared to 2006 from TOAR measurements (magenta line), due to changes in bottom-up NO$_x$ emissions (black), due to changes in top-down NO$_x$ emissions (blue lines for simulations from GC-adj and red lines for simulations from GCv12), and due to changes in meteorology and non-NO$_x$ emissions (green line). Only sites that have continuous measurements throughout the 9 years are included. The vertical bars represent the spread of changes from simulations using the NASA and the DOMINO posterior NO$_x$ emissions. The impact of meteorology and natural sources are removed from black, blue and red lines by subtracting simulations using 2010 bottom-up anthropogenic emissions for all years from simulations that use bottom-up NO$_x$ emissions corresponding to each year.

Atmospheric
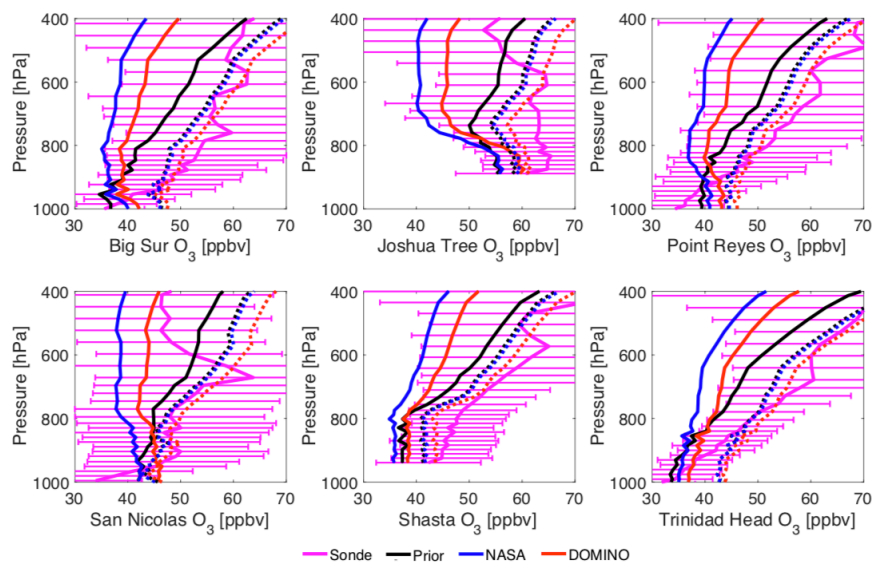Chemistry
and Physics
Discussions
Open Access
EGU

Figure 10. Ozone vertical profiles averaged over May and June of 2010 from 6 ozonesonde measurement sites from the IONS-2010 field experiment in California. Solid black (prior), blue (NASA posterior) and red (DOMINO posterior) lines are from the GCv12 simulations (prior anthropogenic emission from CEDS), whereas dashed lines are from the GC-adj simulations (prior anthropogenic emission from HTAP). The horizontal bars show the standard deviations of the measurements at each vertical layer.
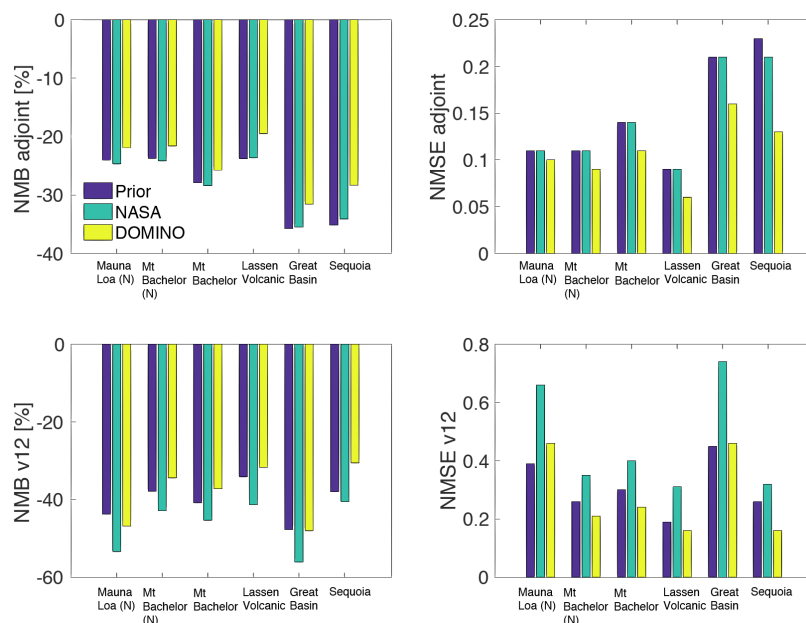
Figure 11. NMSE and NMB of GC-adj (top) and GCv12 (bottom) ozone simulations in 2010 –2014 evaluated with surface measurements at remote sites. Three sets of NO$_x$ emissions, i.e., bottom-up inventory (HTAP for GC-adj, CEDS for GCv12), DOMINO posterior, and NASA posterior, are input in each model.